Applied Catalysis B: Environmental 181 (2016) 825–837

Contents lists available at ScienceDirect

Applied Catalysis B: Environmental

journal homepage: www.elsevier.com/locate/apcatb

Photocatalytic activity and luminescence properties of RE^{3+}–TiO_2 nanocrystals prepared by sol–gel and hydrothermal methods

Joanna Reszczyńska[a,b,c,*], Tomasz Grzyb[d], Zhishun Wei[c], Marek Klein[a,e], Ewa Kowalska[c], Bunsho Ohtani[c], Adriana Zaleska-Medynska[a,b]

[a] Department of Chemical Technology, Faculty of Chemistry, Gdansk University of Technology, 80-233 Gdansk, Poland
[b] Department of Environmental Engineering, University of Gdansk, 80-308 Gdansk, Poland
[c] Catalysis Research Center, Hokkaido University, Sapporo 001-0021, Japan
[d] Department of Rare Earths, Faculty of Chemistry, Adam Mickiewicz University, 60-780 Poznan, Poland
[e] Institute of Fluid-Flow Machinery, Polish Academy of Sciences, 80-231 Gdansk, Poland

ARTICLE INFO

Article history:
Received 22 June 2015
Received in revised form 31 August 2015
Accepted 2 September 2015
Available online 7 September 2015

Keywords:
TiO_2
Heterogeneous photocatalysis
The sol–gel method
Hydrothermal method
Rare earth metal

ABSTRACT

A series of Y^{3+}, Pr^{3+}, Er^{3+} and Eu^{3+} modified TiO_2 photocatalysts were obtained via sol–gel (SG) and hydrothermal (HT) methods. Samples prepared this way were characterized by X-ray powder diffractometry (XRD), X-ray photoelectron spectroscopy (XPS), diffuse reflectance spectroscopy (DRS), scanning transmission microscopy (STEM), BET surface area method and luminescence spectroscopy. The photocatalytic activity of the synthesized samples was evaluated by the degradation of phenol in aqueous solution under visible and ultraviolet light irradiations. Phenol in aqueous solutions was successfully decomposed under visible light ($\lambda > 420$ nm) using TiO_2 modified with RE ions. Luminescence properties of the samples as well as XRD and XPS analyses, indicate that RE are rather in the form of their oxides than in the form of cations in the crystal structure of TiO_2. Photocatalysts prepared by SG method possessed higher amount of RE_2O_3, fewer of OH^- groups and Ti^{3+} species on the surface layer than powders obtained by HT method. Action spectra analysis showed that Pr^{3+}-modified TiO_2 could be excited under visible light in the 420–250 nm range. Furthermore, photocatalysts obtained by HT method showed higher photocatalytic activity and lower intensity of luminescence emission than photocatalyst prepared by SG method.

1. Introduction

Heterogeneous photocatalysis, in presence of TiO_2, has been extensively studied for the degradation of hazardous pollutants in air and water under ultraviolet (UV) or solar light for over 40 years [1–8]. When TiO_2 is illuminated by an appropriate range of irradiation, the pairs of electrons and holes are generated inside photocatalyst crystal lattice. The major problem in its practical application is a wide band gap which requires a high energetic UV light for its excitation (e.g., the band gap of anatase form of titania is about 3.2 eV). Therefore, a lot of studies have been performed to develop a photocatalytic system which can be activated under visible light irradiation [9–13].

Recently, it was reported that the loading of rare earth (RE) elements into the semiconductor photocatalysts can alter the surface adsorption properties as well as the complexation of the organic contaminants through their f-orbitals to bring the effective outcome for the environmental remediation [14–16]. Furthermore, modification with RE^{3+} ions prevents electron–hole recombination [17–19].

Several techniques can be used to prepare advanced photocatalytic materials and the sol–gel can be highlighted among all of them [19–22]. Recently, this method has been more and more popular as a straightforward preparation process to produce nanosized crystallized powders of high purity at relatively low temperature. Moreover, it is also applicable in stoichiometry controlling process, preparation of composite or homogeneous materials [23]. Furthermore, the sol–gel method is a cheap, simple and reproducible way of synthesis [24]. The key feature is that luminescence properties of RE^{3+} depend on the variations in the network at the vicinity of ion. The sol–gel method, especially followed by annealing process, allows for the synthesis of RE^{3+}-modified mate-

* Corresponding author at: Department of Environmental Engineering, University of Gdansk, 80-308 Gdansk, Poland.
E-mail address: joanna.reszczynska@ug.edu.pl (J. Reszczyńska).

http://dx.doi.org/10.1016/j.apcatb.2015.09.001
0926-3373/

rials with the relatively low contamination by organic residues. Moreover, higher crystallinity of RE^{3+} host material obtained by applying thermal post-treatment, results in lowered effectiveness of quenching processes and thus improves luminescence. Therefore, the method of RE^{3+}–TiO_2 preparation may have different influences on luminescence properties [25]. In our previous work, novel TiO_2 photocatalysts prepared by the sol–gel method and modified with Er^{3+}/Yb^{3+}, Nd^{3+}/Er^{3+}, Nd^{3+}/Eu^{3+}, Eu^{3+}/Ho^{3+} showed high photocatalytic activity and low RE^{3+} luminescence intensity [24,26]. On the other hand, the materials obtained by hydrothermal treatment tend to have greater stability against unwanted crystalline phase transformation (from anatase to rutile) and crystal growth [27,28]. This can affect the intensity of the luminescence and photocatalytic activity of powders.

It was reported that properties of titania obtained by sol–gel and hydrothermal methods differed significantly i.e., hydrothermal process resulted in formation of more uniform particles in size [29].

In this context, we have recently obtained TiO_2 modified with Pr^{3+}, Eu^{3+}, Er^{3+}, Y^{3+} using two different preparation routes, such as sol–gel and hydrothermal methods. In this paper, we present the effect of the preparation method on the surface features, luminescence properties as well as UV–vis and vis ($\lambda > 420$ nm) driven photocatalytic activity. For the first time, photocatalytic activity of RE–TiO_2 (RE = Pr, Eu, Er and Y) is correlated with preparation route, and thus with surface properties. Furthermore, the mechanism of UV and visible light excitation of as prepared RE–TiO_2 obtained by two different routes is proposed and discussed.

2. Experimental

2.1. Materials and apparatus

Titanium isopropoxide (97%, TIP) was purchased from Sigma–Aldrich and used as titanium source for the preparation of TiO_2 nanoparticles. $Pr(NO_3)_3{\cdot}6H_2O$, $Eu(NO_3)_3{\cdot}6H_2O$, $Er(NO_3)_3{\cdot}6H_2O$, $Y(NO_3)_3{\cdot}6H_2O$ were obtained from Sigma–Aldrich, acetic acid and ethanol from Poch S.A. Poland, while TiO_2 P25 from Evonik, Germany (surface area: ca. 50 m^2/g, crystalline composition: 73–85% anatase, 14–17% rutile and 0–13% amorphous titania [30]). Acetic acid was added in order to control hydrolysis and condensation reactions, and to obtain pure anatase phase [31]. All the chemicals were used as received without further purification. Deionized water was used for all the reactions and treatment processes.

To characterize the absorption properties of modified photocatalysts, diffuse reflectance (DR) spectra were recorded and data were converted by K–M function to obtain absorption spectra. The measurements were carried out on UV–vis Thermo model: Nicolet Evolution 220 with ISA-220 integrating sphere. $BaSO_4$ was used as the reference.

Nitrogen adsorption–desorption isotherms were recorded at liquid nitrogen temperature (−197 °C) on a Micromeritics Gemini V (model 2365) and the specific surface areas were determined by the Brunauer–Emmett–Teller (BET) method in the relative pressure (p/p_0) range of 0.05–0.3. All the samples were degassed at 200 °C prior to nitrogen adsorption measurements.

The morphology RE^{3+}–TiO_2 was observed by scanning transmission electron microscopy (STEM; HITACHI HD2000) with the accelerating voltage and emission current of 200 kV and 30 μA, respectively. Powders were dispersed in ethanol in an ultrasonic bath for a few minutes, and then droplet of suspension was deposited on a carbon-covered copper microgrid which was dried under vacuum overnight. Images were acquired at a wide range of magnifications (50,000–800,000) at the normal resolution, at a working distance of 3 mm as secondary electron (SE), Z-contrast (ZC), and bright-field (BF) modes.

The samples were also characterized by scanning electron microscopy with energy dispersive X-ray spectroscopy (SEM/EDS; JEOL JSM-6360LA/JED-2300) using a Mg Kα X-ray source. The accelerating voltage and the working distance were kept at 20 kV and 10 mm, respectively. Each sample was analyzed for five different area and average data were used for composition determination.

X-ray diffraction (XRD) patterns were recorded on a diffractometer (Rigaku, RINT Ultima+) equipped with a graphite monochromator using copper Kα radiation (40 kV tube voltage and 20 mA tube current) in $2\theta = 5$–90°. To determine primary particle sizes of photocatalysts, XRD data were calculated using Scherrer's equation.

X-ray photoelectron spectroscopy (XPS) measurements were carried out on JEOL JPC-9010MC spectrometer using monochromatic Mg Kα X-rays source. For determination of Ti, O and C elements, 20 scans were carried out and average data were used for analysis. Considering the low content of RE elements, 50 scans were performed for analysis of Y, Pr, Er and Eu. During measurements, pressure in the main chamber was kept below 5.0×10^{-6} Pa.

Spectroscopic properties (emission and luminescence lifetimes) were measured on Quanta Master™ 40 spectrophotometer equipped with Opolette 355LD UVDM tunable pulsed laser as an excitation source with the repetition rate 20 Hz (pulse length 7 ns) and a Hamamatsu R928 photomultiplier as a detector. All of the measurements were carried out using powdered samples dried and grounded in mortar before the experiment.

2.2. Preparation of RE^{3+}–TiO_2 photocatalysts

RE–TiO_2 samples were prepared by two methods, i.e., hydrothermal (HT) and sol–gel (SG). Crystallization of titania was performed at temperature of 400 °C for 2.5 h in the air. Thus, obtained samples were labeled as TiO_2_RE(molar concentration of RE to TiO_2)_(method of preparation), e.g., TiO_2_Y(0.25)_HT indicates that the Y modified titania sample (0.25 mol.% as for Y) was prepared under hydrothermal reaction. For comparison, the TiO_2 nanocrystals without any RE ions were also synthesized under the same preparation process and sample were labeled as TiO_2_Pure_SG and TiO_2_Pure_HT. The description of the prepared photocatalysts is shown in Table 1. HT and SG methods are briefly described in the following sections.

2.2.1. Hydrothermal method

In typical procedure, 6 mL of TIP was dissolved in solution of 24-mL ethanol and 2.4-mL acetic acid (solution A), and stirred for 10 min. Then 30 mL of water was added to certain amount of solid rare earth nitrate ($Pr(NO_3)_3{\cdot}6H_2O$, $Eu(NO_3)_3{\cdot}6H_2O$, $Er(NO_3)_3{\cdot}6H_2O$, $Y(NO_3)_3{\cdot}6H_2O$) and the pH of the solution was adjusted at 2.5 with HNO_3 (solution B). In the next step, the solution B was dropped into the solution A and obtained sol was stirred for one more hour. After treatment at 160 °C for 48 h in an autoclave (hydrothermal process), the as-obtained samples were separated by centrifugation, washed four times with deionized water, dried at 80 °C and grounded to obtain uniform powders.

2.2.2. The sol–gel method

In the first step, 15 mL of TIP was dissolved in solution of 60-mL ethanol and 6-mL acetic acid and stirred for 10 min. In the next step, 14 mL (pH 2.5 adjusted with HNO_3) of deionized water was dropped into the solution under vigorous agitation. Then, a certain amount of rare earth nitrate ($Pr(NO_3)_3{\cdot}6H_2O$, $Eu(NO_3)_3{\cdot}6H_2O$, $Er(NO_3)_3{\cdot}6H_2O$, $Y(NO_3)_3{\cdot}6H_2O$) was dissolved in 2 mL of water, and

Table 1
Description and physicochemical characterization of RE^{3+}–TiO_2 photocatalysts synthesized by hydrothermal and sol–gel methods.

Sample label	Preparation method	Metal precursor used during preparation	Assumed content of RE (mol.%)	Crystals size (nm)	S_{BET} (m^2/g)
TiO_2_Pure_HT	Hydrothermal	None	None	9.3	118
TiO_2_Y(0.25)_HT	Hydrothermal	$Y(NO_3)_3{\cdot}6H_2O$	0.25	9.4	120
TiO_2_Pr(0.25)_HT	Hydrothermal	$Pr(NO_3)_3{\cdot}6H_2O$	0.25	9.0	127
TiO_2_Er(0.25)_HT	Hydrothermal	$Er(NO_3)_3{\cdot}6H_2O$	0.25	8.9	127
TiO_2_Eu(0.25)_HT	Hydrothermal	$Eu(NO_3)_3{\cdot}6H_2O$	0.25	8.6	133
TiO_2_Pure_SG	Sol–gel	None	None	9.9	117
TiO_2_Y(0.5)_SG	Sol–gel	$Y(NO_3)_3{\cdot}6H_2O$	0.5	8.8	151
TiO_2_Y(0.25)_SG	Sol–gel	$Y(NO_3)_3{\cdot}6H_2O$	0.25	8.5	130
TiO_2_Pr(0.5)_SG	Sol–gel	$Pr(NO_3)_3{\cdot}6H_2O$	0.5	9.1	134
TiO_2_Pr(0.25)_SG	Sol–gel	$Pr(NO_3)_3{\cdot}6H_2O$	0.25	9.2	127
TiO_2_Er(0.5)_SG	Sol–gel	$Er(NO_3)_3{\cdot}6H_2O$	0.5	9.1	132
TiO_2_Er(0.25)_SG	Sol–gel	$Er(NO_3)_3{\cdot}6H_2O$	0.25	8.5	112
TiO_2_Eu(0.5)_SG	Sol–gel	$Eu(NO_3)_3{\cdot}6H_2O$	0.5	8.8	133
TiO_2_Eu(0.25)_SG	Sol–gel	$Eu(NO_3)_3{\cdot}6H_2O$	0.25	9.2	131

the sol was stirred for one more hour. As-obtained gel was dried at 80 °C and grounded to obtain powders.

2.3. Photoactivity tests

Photoactivity of samples was measured for two reaction systems, i.e., under polychromatic and monochromatic irradiation to check overall activity of samples and to calculate quantum efficiency, respectively. Polychromatic irradiation was carried out for two irradiation ranges, i.e., full-spectrum (UV–vis) and cut-off spectrum (vis) of light.

2.3.1. Phenol decomposition under polychromatic irradiation

Irradiation experiments were carried out under UV and/or vis using a xenon lamp (Xe emission lamp range: 250–1100 nm). A rare earth metal modified photocatalyst (125 mg) was suspended in 0.21 mM phenol aqueous solution (25 mL), which was selected as a model contaminant. The suspension was placed in a quartz photoreactor. After 30-min aeration (5 dm^3/h), the suspension was irradiated with a Xenon 1000 W lamp. The optical path included a water filter to cut off IR irradiation. For the test of visible light-induced activity the light beam passed through GG420 filter to cut-off wavelengths shorter than 420 nm. One-milliliter aliquots of the aqueous suspension were collected at regular time periods during irradiation and filtered through syringe filters (Ø = 0.2 mm) to remove photocatalyst particles. Phenol concentration was estimated by the colorimetric method (λ = 480 nm) after derivatisation with diazo-*p*-nitroaniline using UV–vis spectrophotometer (DU-520, Beckman). Phenol photodegradation followed a pseudo-first-order kinetics and the photocatalytic activity was presented as phenol rate constant (h^{-1}). To investigate the adsorption properties of prepared samples, adsorption tests of phenol were performed for 1 h stirring in the dark (0.21 mM, 25 mL phenol aqueous solution, 125 mg photocatalyst).

2.3.2. Acetic acid decomposition-action spectra measurements

For the selected photocatalysts the action spectra measurements were investigated. Photocatalyst (30 mg) was suspended in an aqueous solution (3.0 mL) of 5-vol% acetic acid, the suspension was placed in a rectangular quartz cell (10 mm square and 50 mm in height), and irradiated with monochromatic light for 150 min using a diffraction grating-type illuminator (Jasco, CRM-FD) equipped with a 300 W Xenon lamp (Hamamatsu, C2578-02). The light intensity was measured by an optical power meter (HIOKI 3664). During the experiments, the reaction mixtures were continuously stirred. Every 20 min of irradiation, 0.2-mL portion of the gas phase of the reaction mixture was withdrawn with a syringe and subjected to gas chromatographic analysis of carbon dioxide (Shimadzu GC-8A). The wavelength-dependent apparent quantum efficiency was calculated as the ratio of electron consumption (from the rate of CO_2 generation) and the flux of incident photons, assuming that four photons are required, according to the stoichiometry of the reaction:

$$CH_3COOH + 2O_2 = 2CO_2 + 2H_2O$$

3. Results and discussion

The description of all samples prepared this way,including preparation methodology and selected surface properties, are summarized in Table 1.

3.1. Diffuse reflectance spectroscopy

To study the optical absorption properties of bare and modified titania samples, the diffuse reflectance spectra (DR) were investigated in the range of 350–700 nm. Obtained data are shown in Fig. 1. P25 was chosen as a reference sample and it clearly shows absorption only in the UV region. All prepared powders were white. All modified powders showed a slight shift of their absorption edge into the visible light compared to P25. Comparing with unmodified TiO_2 prepared by HT method, a tiny blue-shift of the absorption profile was observed for all modified samples in Fig. 1. This behavior is very similar to the previously reported results [32], where broadening of band gap was observed after titania modification with Eu. It was proposed that the gradual movement of the conduction band of TiO_2 above the first excited state of Eu^{3+} was the possible reason of such band gap energy increase. Incorporated Eu^{3+} ions at the first excited state could interact with the electrons of the conduction band of TiO_2, resulting in a higher energy transfer from TiO_2 to Eu^{+3} ions. Moreover, the blue-shift might be also ascribed to quantum size effect, due to the decrease of the crystalline size [33]. Pure TiO_2 was obtained using the same method as the modified one, thus stronger absorption observed for pure TO_2 (SG) could be related to the presence of impurities originating from reaction reagents (such as acetic acid) and incorporated during synthesis into TiO_2 structure [24]. The DR results showed that when the HT method was applied then the optical absorption edge was shifted more to the red direction. Moreover, the increasing amount of Er^{3+}, Eu^{3+}, Pr^{3+} used for modification resulted in larger shift of absorption edge towards to longer wavelength. The absorption peaks at 452, 477, 524 and 655 nm are characteristic for erbium element and could be identified with the transition from the $^4I_{15/2}$ ground state to the excited states of erbium ions $^4F_{3/2,5/2}$, $^4F_{7/2}$, $^2H_{11/2}$ and $^4F_{9/2}$ [34–36]. Furthermore, the absorption peaks located at 446, 470, 486 and 592 nm could be attributed to the transition from $^3H_4$ ground state to the excited states of the praseodymium ions $^3P_2$, $^3P_1$, $^3P_0$ and $^1D_2$ [37–39]. The intensity of absorption bands

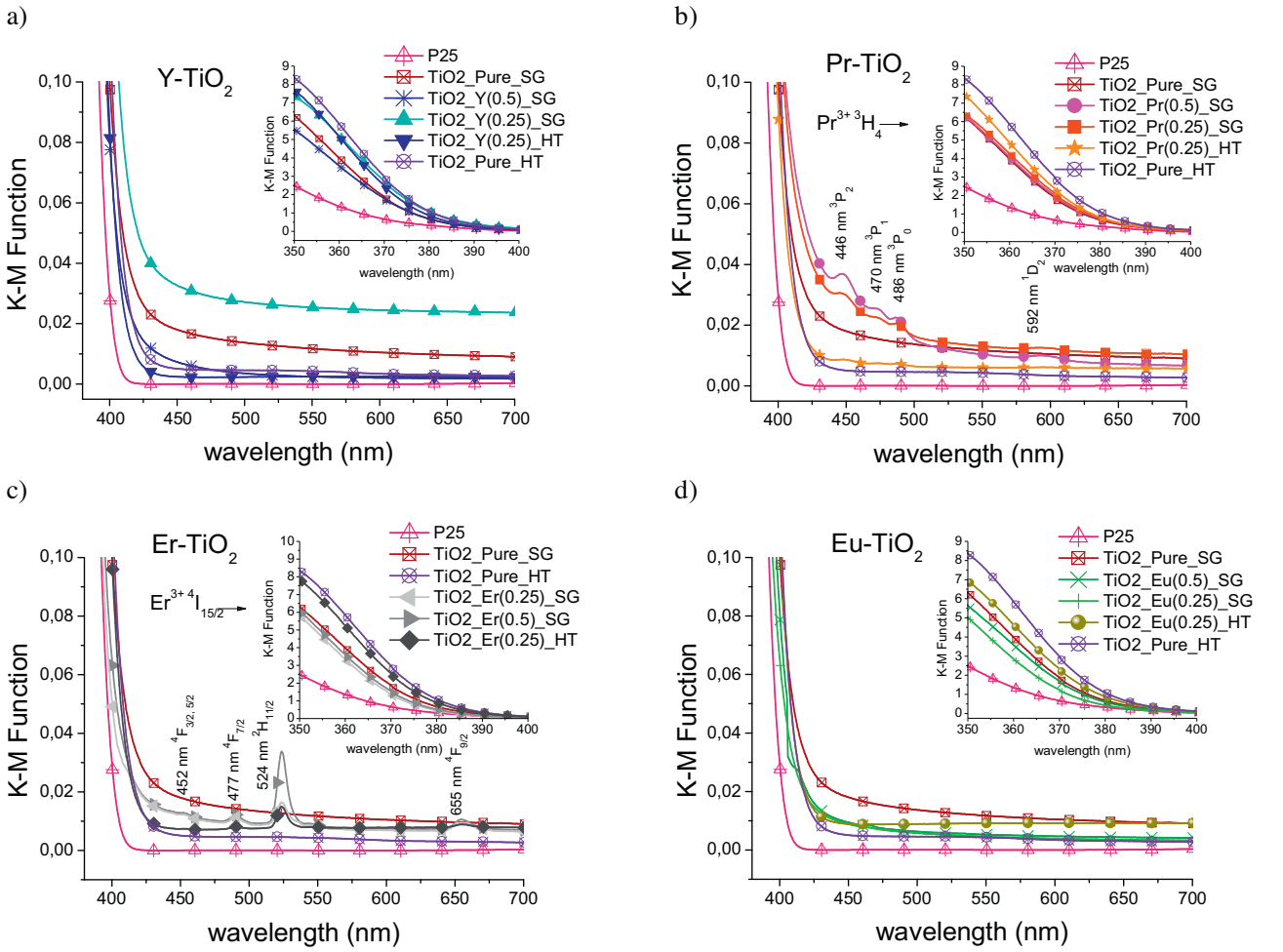

Fig. 1. UV–vis Kubelka–Munk absorption of RE^{3+}–TiO_2 photocatalysts compared to P25 and pure TiO_2 (a) Y–TiO_2; (b) Pr–TiO_2; (c) Er–TiO_2; (d) Eu–TiO_2. (For interpretation of the references to color in the text, the reader is referred to the web version of this article.)

of erbium and praseodymium ions increased with increasing the RE content. According to Judd–Ofelt theory of parity-forbidden electric-dipole transitions of rare earth ions, the energy states of Er^{3+} should be effectively perturbed by the odd terms of the Hamiltonian of the weak crystal field. Although 4f energy electrons have been partially screened by $5s^2$ and $5p^6$ electron shells, the perturbations can still cause permitted transitions of 4f elections between 4f energy levels [40]. The transitions of 4f electrons of Er^{3+} favor the separation of photogenerated electron–hole pairs being helpful for the improvement of photocatalytic activity under visible and UV light [41].

3.2. Nitrogen and phenol adsorption

The specific surface areas (determined by nitrogen adsorption, BET method) of bare and RE metal modified TiO_2 photocatalysts are listed in Table 1. As showed in Table 1, the BET surface areas of the modified samples were higher than those of the pure TiO_2 samples, except, the surface area of TiO_2 Er(0.25) SG. The introduction of Er ions increased the specific surface area of TiO_2 HT from 118 to 127 m^2/g, but decreased the specific surface area of TiO_2 SG from 117 to 112 m^2/g. The highest BET surface area was observed for TiO_2_Y(0.5)_SG sample (151 m^2/g). The BET surface areas for photocatalysts modified with Er^{3+} and Eu^{3+} by HT method were higher than those of the powders obtained by SG method. An increase in the RE content from 0.25 to 0.5 mol.% caused an increase in the BET surface area. These results are compatible with the literature reported previously [26,39,42]. To investigate the adsorption properties of pure and RE^{3+} modified TiO_2 photocatalysts, tests of phenol adsorption were performed in the dark. The reference experiments in the dark showed that phenol did not adsorb on pure and modified titania photocatalysts.

3.3. X-ray powder diffraction method

The XRD patterns of pure TiO_2 and RE^{3+}–TiO_2 samples are shown in Fig. 2. Observed XRD peaks can be assigned to the (1 0 1), (0 0 4), (2 0 0) and (1 0 5) facets of anatase, where the most intense (1 0 1) peak appears at $2\theta = 25.4^\circ$ [43]. The phase transformation to rutile did not occur, despite heat treatment at 400 °C. Refraction of RE oxide, such as Y_2O_3, Pr_2O_3, Er_2O_3 or Eu_2O_3, was not observed in the XRD patterns, indicating that either (i) the content of RE oxides was below detection limit, (ii) crystalline sizes were too small to be detected, (iii) amorphous, but not crystalline oxides were formed, or (iv) RE cations were placed inside titania lattice (titania doping). The slight broadening of diffraction peaks indicates formation of small sized nanocrystals. The structural refinement has revealed that the anatase crystallite size and the lattice strain of modified samples slightly decreased in comparison to pure titania, e.g., crystalline size decreased from 9.9 nm to 8.5 after TiO_2_Pure_SG modification with 0.25 mol.% of Er (Table 1). RE^{3+}–TiO_2 photocatalysts prepared by HT method showed higher contraction of unit cell parameters than that obtained by SG method. Decrease in content of RE elements (from 0.5 to 0.25 mol.%) resulted in increase in the

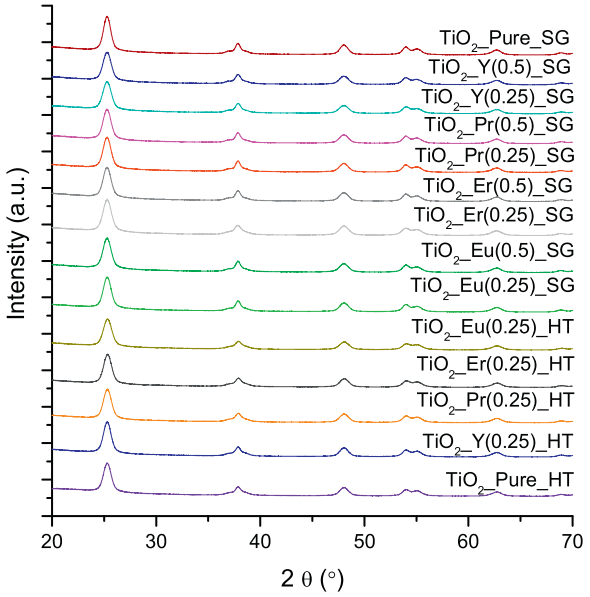

Fig. 2. XRD pattern of RE–TiO_2 photocatalysts prepared by sol–gel and hydrothermal methods.

contraction of the unit cell (Table 2). Our findings correlate with some literature reports [42]. It is known that the ionic radiuses of Y^{3+} (93 pm) [44], Pr^{3+} (99 pm) [45], Eu^{3+} (95 pm) [6] and Er^{3+} (88 pm) [26] are larger than that of Ti^{4+} (61 pm) [26], which should result in lattice expansion as RE^{3+} incorporates into the TiO_2 crystal lattice. However, no lattice expansion is observed for all modified samples, demonstrating that RE^{3+} species exist at the crystal boundary rather than in the inner crystalline structure of TiO_2. Consequently, it is very probable that the surrounding RE ions are incorporated into Ti–O–RE structures formed at the crystal boundary of anatase TiO_2, which inhibit the phase transformation from anatase to rutile and the crystallite growth by restricting direct contact of crystallites [46]. The BET and XRD analyses showed that RE^{3+}-modification caused increase in specific surface area, probably due to preparation of smaller crystallites of titania. However, the lack of linear correlation between crystalline size of titania and specific surface area suggests another reason of BET increase, e.g., that small nanoparticles of oxides (RE_2O_3) were formed on the surface of TiO_2 nanocrystals resulting in increase in specific surface area. An increase in specific surface area with increase in RE content for all modified samples indicate high probability of this hypothesis.

3.4. Scanning transmission microscopy and Energy-dispersive X-ray spectroscopy analysis

The morphology of all tested samples practically did not differ and deposits of RE oxides were not observed by any of used STEM modes (SE, TE and ZC). It was found that SG and HT syntheses resulted in preparation of titanias of almost the same morphology, as shown in Fig. 3. The particle size varied from 5 to 15 nm correlating well with crystalline sizes determined by XRD, which indicates that single crystals dominate in RE-titania photocatalysts (only a few aggregates of larger sizes of 50–100 nm were observed).

Energy-dispersive X-ray spectroscopy (EDX) was performed for characterization of titania modified by 0.5 mol.% of RE. The presence of RE elements was confirmed in all tested samples, but determined amount of RE element varied from 0.12 to 0.51 mol.%, which was caused by low precision of EDX analysis for components of small content (RE) in the sample. Atomic ratios of O to Ti were much smaller than expected from molecular formula of TiO_2(2) and equaled to 1.64, 1.05, 0.87 and 1.01 for Y-, Pr-, Er- and Eu-modified titania, respectively which was caused by limitation of EDX to elements of large atomic number (low yield of X-ray absorption by light elements like oxygen). Even if quantitative analyses were not precise, the oxygen distribution correlated with SEM image indicating its uniform distribution on the surface of sample (Fig. S1 in the Supplementary material).

Table 2
Unit cell parameters for selected samples.

Sample label	*a* (Å)	*c* (Å)	*V* (Å^3)
TiO_2_Pure_HT	3.7857(5)	9.4977(12)	136.120
TiO_2_Y(0.25)_HT	3.7833(6)	9.4921(14)	135.868
TiO_2_Pr(0.25)_HT	3.7830(4)	9.4909(12)	135.828
TiO_2_Er(0.25)_HT	3.78141(16)	9.4870(5)	135.656
TiO_2_Eu(0.25)_HT	3.78233(18)	9.4875(5)	135.729
TiO_2_Pure_SG	3.7856(5)	9.5016(13)	136.169
TiO_2_Y(0.5)_SG	3.7844(6)	9.4977(14)	136.028
TiO_2_Y(0.25)_SG	3.7845(2)	9.4953(6)	135.998
TiO_2_Pr(0.5)_SG	3.7850(2)	9.4983(6)	136.077
TiO_2_Pr(0.25)_SG	3.7843(2)	9.4961(6)	135.995

3.5. X-ray photoelectron emission spectroscopy

The composition of surface layer of RE-modified titania was studied by XPS. Four main elements were analyzed in details by narrow XPS scanning, i.e., titanium, oxygen, carbon and RE-element and results are summarized in Table 3. All samples contained excess of carbon on the surface (20–45 %), which could result from organic precursor (TIP), acetic acid and ethanol used for titania hydrolysis. Birnie and Bendzko [47] suggested that titanium isopropoxide could exchange isopropyl groups with modifying acetate groups to form $Ti(OiPr)_2(OAc)_2$ molecule. Titanium carboxylates have high thermal stability and this could be the reason of high amount of carbon in TiO_2 surface layer [48]. The atomic ratio of oxygen to titania depended on the kind of RE. It was found that modification of titania with Er and Eu resulted in two or slightly higher ratios indicating well crystallized titania enriched with hydroxyl group on the surface. However, bare titanias and modified with Y and Pr exhibited a lack of oxygen (O:Ti < 2) indicating either the presence of crystal lattice defects (oxygen vacancies) or substitution of surface oxygen with RE confirming the hypothesis (XRD data) that RE are placed mainly on the surface of titania. After deconvolution of titanium and oxygen peaks (Fig. 4) it was found that titanium in bare and Y-modified samples existed mainly in Ti^{+4} form (80–83 %) independently on Y content, as shown in Table 4. Oxygen states varied for all tested samples. O 1s region could be de-convoluted for two to three peaks at BE of 529.2–529.4 eV, 529.8–531.2 eV and 532.1–532.9 eV. The first peak can be attributed to TiO_2, the second peak to OH^- group binding with two Ti atoms, Ti_2O_3 or Y_2O_3 [49,50], the third peak to surface oxygen in Ti–OH [24]. In comparison with our previous data for bimetallic-modified titania with Nd/Er, Nd/Eu and Eu/Ho (9–90%) [24], much lower amount of oxygen in the form of surface hydroxyl group was found after modification with Y (3–14%, but even 90% for Nd/Er [24]). This could result from applied conditions of thermal treatment, i.e., lower temperature and shorter time, probably insufficient for surface enrichment with oxygen. It is important to mention that position of titanium peak after modification with RE elements did not change, which once again indicates the surface modification rather than substitution of titanium lattice by RE. Thus, it is possible that either an interstitial doping or surface modification of titania by small clusters of RE oxides took place.

3.6. Luminescence spectroscopy

Spectroscopic properties of prepared samples are presented in Figs. 5 (a and b) and 6 (a and d). Under excitation by UV light

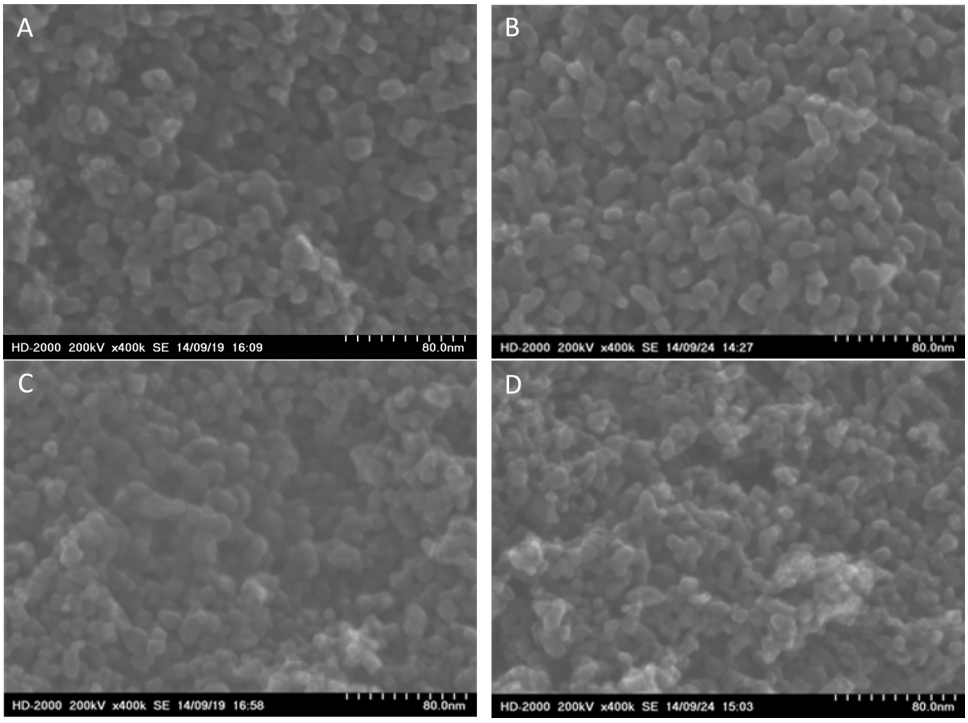

Fig. 3. STEM images of (A) TiO_2_Pure_HT; (B) TiO_2_Pure_SG; (C) TiO_2_Er(0.25)_HT; (D) TiO_2_Y(0.5)_SG.

($\lambda = 355$ nm) TiO_2 and RE^{3+}–TiO_2 showed a weak broad emission band with maximum intensity at around 425–450 nm (Fig. 5). The observed emission was associated with recombination of charge carriers, i.e., electrons and holes [51]. The maximum of the emission peak depends on the type of recombination taking place as well as method of synthesis and could shift from the red to blue spectral range [51,52].

The emission seems to be independent on the type of RE^{3+}-element however, it is worth noting that bare and Er^{3+}-modified (0.25%) samples prepared by SG method showed the highest luminescence intensity. Materials prepared by HT method showed lower emission intensity than those obtained by a SG technique, despite the fact that absorption in the UV range was higher in the case of hydrothermally prepared materials. This indicates that HT method caused preparation of titania particles with lower content of recombination centers. In this regard, higher level of photocatalytic activity is expected for those samples prepared by HT method, as will be discussed later.

The presence of lanthanide ions (Ln^{3+}) in the structure of material can be confirmed by luminescence spectroscopy. As it is well known, Ln^{3+} ions show characteristic and typical lines for each ion in their luminescence spectra (except La^{3+} and Lu^{3+} which have empty or filled 4f sub-shell). These properties result from f–f transitions in the electronic 4f shell of Ln^{3+} ions. Because of relative low sensitivity of the f–f electronic transitions on the Ln^{3+} local environment, emission bands observed on the spectra are usually narrow and sharp, with the typical, almost never shifted wavelength of their maxima, and can be treated as fingerprints of the Ln^{3+} ion. However, intensities of some of the Ln^{3+} transitions are sensitive on the configuration of the local environment and may change, depending on the local symmetry of surrounding ions. This property is useful for tracking the structural changes. Especially Eu^{3+} ions were widely used for this purpose [53]. Additional information can be obtained from luminescence decays. The characteristics of the registered curve depend on the quenching processes taking place in the studied material, as well as the number and symmetry of sites occupied by dopant ions.

From the used dopant ions: Y^{3+}, Pr^{3+}, Er^{3+} and Eu^{3+}, the first one is spectroscopically neutral because in the Y^{3+} electronic structure there is no electrons which can be excited by the radiation from

Table 3
Chemical composition of RE^{3+}–TiO_2 photocatalysts based on XPS analysis.

Sample label	Ti (mol.%)	O (mol.%)	O:Ti	C (mol.%)	C:Ti	RE (mol.%)	RE:Ti
TiO_2_Pure_HT	29.36	46.94	1.6	23.7	0.8	None	None
TiO_2_Y(0.25)_HT	28.46	50.29	1.8	21.18	0.7	0.07	0.0025
TiO_2_Pr(0.25)_HT	25.23	46	1.8	28.1	1.1	0.67	0.0266
TiO_2_Er(0.25)_HT	19.72	43.04	2.2	37.2	1.9	0.05	0.0025
TiO_2_Eu(0.25)_HT	21.01	41.77	2	36.8	1.7	0.54	0.0257
TiO_2_Pure_SG	29.76	50.48	1.7	19.77	0.7	None	None
TiO_2_Y(0.5)_SG	27.5	49.38	1.8	22.98	0.8	0.14	0.0051
TiO_2_Y(0.25)_SG	27.77	50.55	1.8	21.63	0.8	0.05	0.0018
TiO_2_Pr(0.5)_SG	27.14	47.88	1.8	24.09	0.9	0.88	0.0324
TiO_2_Pr(0.25)_SG	25.25	46.96	1.9	26.95	1.1	0.84	0.0333
TiO_2_Er(0.5)_SG	23.75	45.84	1.9	30.3	1.3	0.12	0.0051
TiO_2_Er(0.25)_SG	21.2	42.56	2	36.18	1.7	0.06	0.0028
TiO_2_Eu(0.5)_SG	15.31	39.28	2.6	44.67	2.9	0.73	0.0477
TiO_2_Eu(0.25)_SG	19.5	41.7	2.1	38.24	2	0.57	0.0292

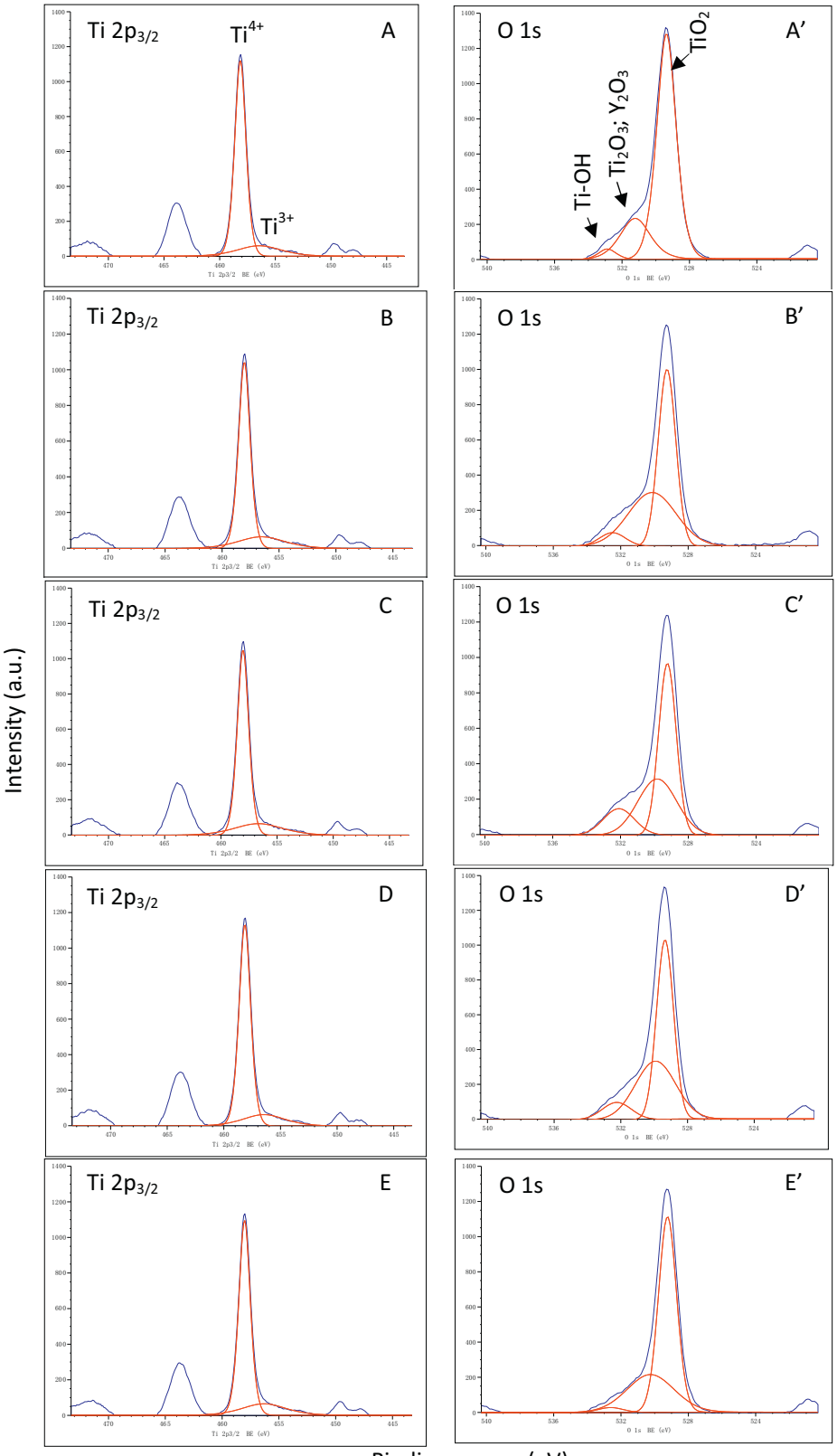

Fig. 4. XPS spectra of prepared photocatalysts—pure and modified by Y–TiO_2.

the ultraviolet to near infrared range (Y^{3+} ion is not an f-element). Therefore, luminescence can be expected only for Pr^{3+}, Er^{3+} and Eu^{3+} ions. These ions can be excited by UV light, but emissions from Pr^{3+} and Er^{3+} ions are usually quenched as the result of their electronic configuration: many of electronic levels separated by relatively small energy gaps. The Eu^{3+} ion can be excited only by the

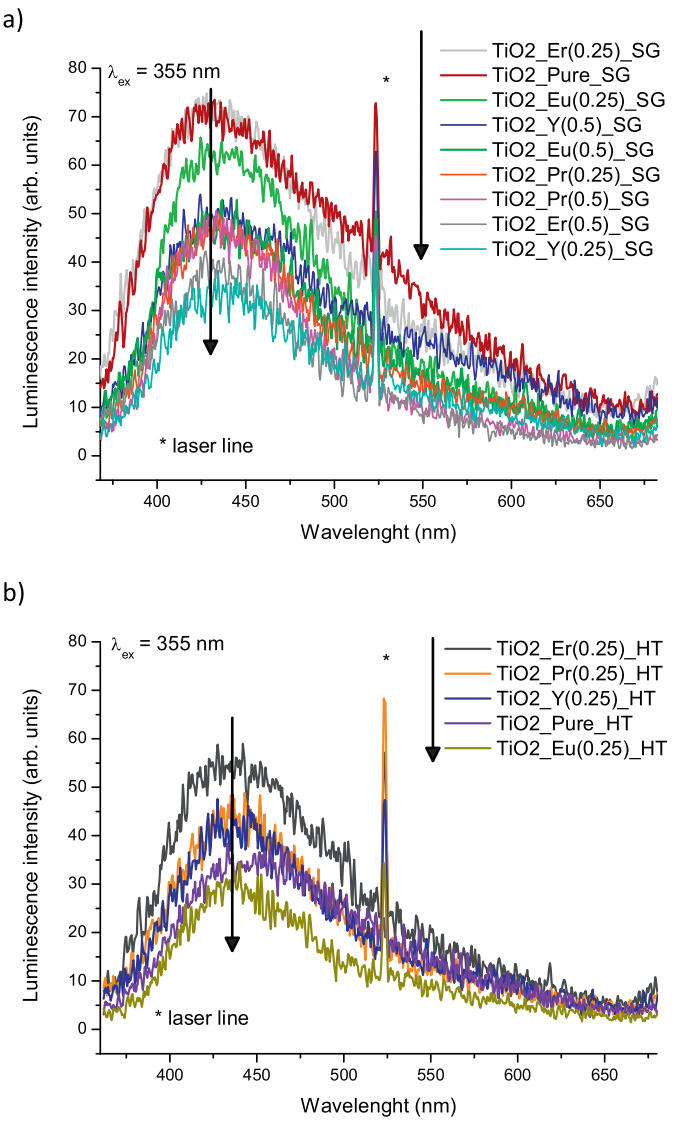

Fig. 5. Emission spectra of prepared photocatalysts under UV light (355 nm)—pure TiO_2 and modified TiO_2 with RE^{3+} by (a) SG method; (b) HT methods.

radiation from the UV–vis range. The most intense luminescence usually is observed after excitation into charge transfer band (when material contain O^{2-} ions) or directly into Eu^{3+} ions (as the result of the excitation from $^7F_0$ ground state to, e.g., $^5L_6$ excited state after absorption of waves with $\lambda \approx 394$ nm). This is caused by the large energy gap between ground and first excited state of Eu^{3+} ions. Both, Pr^{3+} and Er^{3+} ions can be excited by the radiation from the NIR range as the result of sequential absorption of photons (what finally results in up-conversion luminescence).

Modification of TiO_2 with Eu^{3+} ions resulted in a quite intense red luminescence under UV light (250 nm). The spectra showing characteristic emission of Eu^{3+} ions, with transition bands from their $^5D_0$ excited state, are presented in Fig. 6a. Five transition bands were observed: $^5D_0 \rightarrow {}^7F_0$ (577.7 nm), $^5D_0 \rightarrow {}^7F_1$ (588 nm), $^5D_0 \rightarrow {}^7F_2$ (610 nm), $^5D_0 \rightarrow {}^7F_3$ (651 nm) and $^5D_0 \rightarrow {}^7F_4$ (700.2 nm). The observed broad shape of the registered emission bands is typical for disordered systems and is probably caused by multisite distribution of Eu^{3+} ions in the prepared materials. Luminescence intensity from the sample prepared by HT method was around three times lower than that from materials obtained by SG method. Similarly to our previous studies, where the most intense luminescence band was observed for the hypersensitive $^5D_0 \rightarrow {}^7F_2$ transition

Table 4
Chemical composition of pure TiO_2 and Y^{3+}–TiO_2 photocatalysts based on XPS analysis.

Sample label	Ti 2p (%)		O 1s (%)		
	Ti^{+4}	Ti^{+3}	–OH	$Ti_2O_3Y_2O_3$	TiO_2
TiO_2_Pure_HT	81.7	18.3	2.2	32.7	65.1
TiO_2_Y(0.25)_HT	79.7	20.3	13.7	36.2	50.1
TiO_2_Pure_SG	83.3	16.7	8.4	39.6	52.0
TiO_2_Y(0.5)_SG	83.2	16.8	3.3	21.6	75.1
TiO_2_Y(0.25)_SG	80.1	19.9	5.8	42.7	51.5

of Eu^{3+} ions being incorporated into Eu_2O_3 oxide phase [24]. In present report, XPS studies indicate presence of Y_2O_3 phase for the Y^{3+}-modified TiO_2 material. Hence, we can assume that also in the other cases, RE were rather in the form of their oxides, than in the form of cations in the structure of TiO_2.

The characteristics of registered emission spectra were typical for the monoclinic Eu_2O_3 [54]. Emission decays and calculated luminescence lifetimes (Fig. 6c) were typical for Eu^{3+} ions range. The bi-exponential character of luminescence decays results from the multisite distribution of Eu^{3+} ions and the structural properties of Eu_2O_3 oxide, which has two Eu^{3+} sites with different local symmetry. Lifetime values were similar for the both synthesis methods.

Besides Eu^{3+}-modified samples, luminescence was also observed in the case of Er^{3+} containing TiO_2 photocatalysts. Here, the luminescence had different mechanism of excitation, because Er^{3+} ions showed anti-Stokes type emission (up-conversion) [55]. After excitation by near infrared (NIR) laser light, emission spectra composed from $^2H_{11/2} \rightarrow {}^4I_{15/2}$ (~523 nm), $^4S_{3/2} \rightarrow {}^4I_{15/2}$ (~564 nm) and $^4F_{9/2} \rightarrow {}^4I_{15/2}$ (~662 nm) transition bands were registered (Fig. 6b). The observed up-conversion luminescence was very weak. Similar to Eu^{3+}-modified samples, HT method gave a product with lower luminescence intensity. For the excitation, the ground and excited state absorption (GSA and ESA) mechanisms are certainly responsible. To achieve emitting levels of Er^{3+} ions, the sequential absorption of two to three photons is necessary. Luminescence decays of Er^{3+} ions presented in Fig. 6d are short and calculated lifetimes do not exceed 4.7 μs. This is quite low value in comparison to the typical lifetimes of Er^{3+} ions, which are usually in the range of hundreds microseconds [56]. Strongly quenching environment of Er^{3+} ions, i.e., OH^- could be responsible for such short luminescence lifetimes.

Unfortunately for the Pr^{3+}-modified materials, luminescence was not observed after excitation with UV as well as NIR light, due to either its complete quenching or too low intensity of luminescence signal at the noise level.

It should be pointed that TiO_2 material used as host for the RE^{3+} ions is not recommended for applications when effective and intense emission of RE^{3+} ions is needed. In addition, surface properties of titania, and thus method of its preparation, strongly influences the luminescence intensity as was observed by lower effectiveness of Eu^{3+} and Er^{3+} luminescence for samples prepared via HT than SG method. This could be caused by higher amount of hydroxyl group (OH^-, strong luminescence quenchers) on the surface of HT-prepared titania in comparison to these obtained by SG method. The OH^- oscillators are known from their effective quenching properties [57].

3.7. Photocatalytic activity

The photocatalytic efficiency of as-prepared samples was evaluated using aqueous solution of phenol as a model pollutant. Pristine TiO_2 synthesized by the same methods (SG and HT) without RE precursors and P25 were used as a reference samples. Kinetics of phenol photodegradation in an aqueous suspension contain-

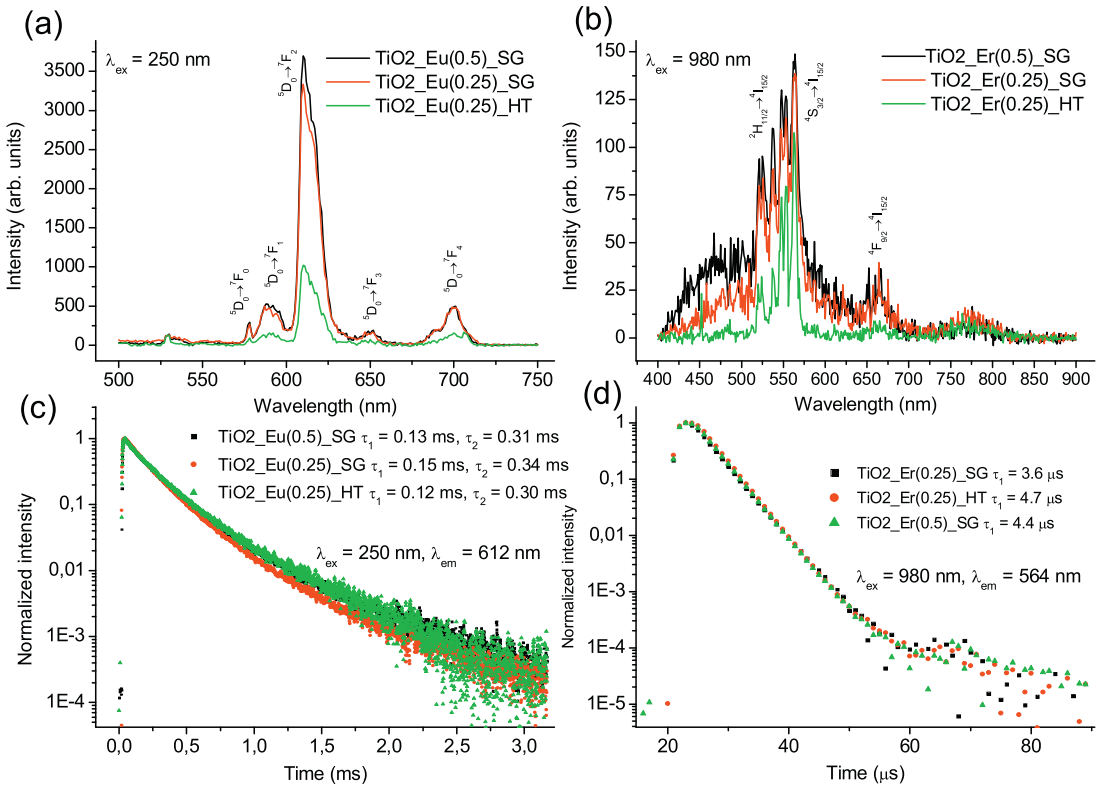

Fig. 6. Luminescence spectra (a and b) and emission decays (c and d) of prepared photocatalysts, under UV (250 nm) and NIR (980 nm) irradiation.

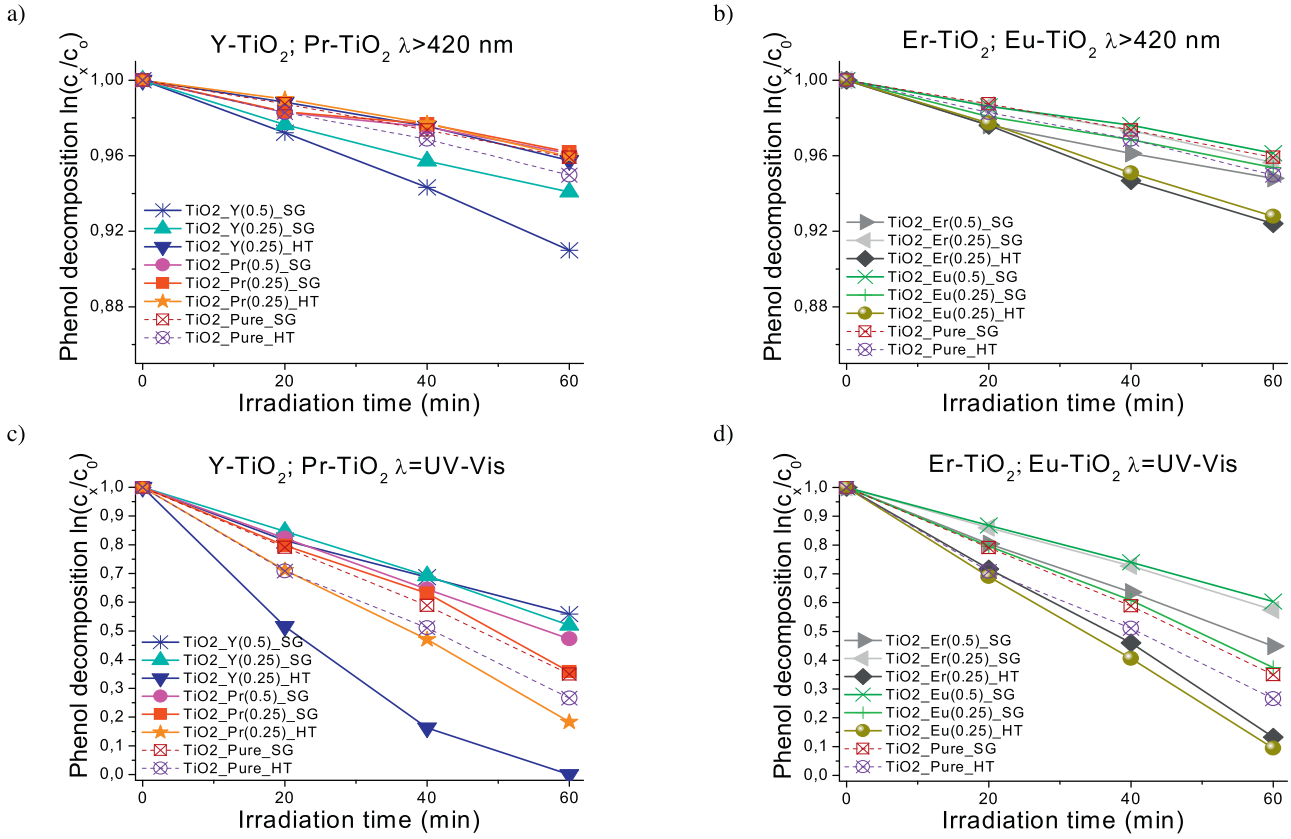

Fig. 7. Photoactivity under UV–vis and vis (λ > 420 nm) light of RE^{3+}–TiO2 (a) vis Y–TiO_2; Pr–TiO_2; (b) vis Er–TiO_2; Eu-TiO2; (c) UV–vis Y–TiO_2; Pr–TiO_2; (d) UV–vis Er–TiO_2; Eu–TiO_2. Experimental conditions: c_0 = 0.21 mM; $m(TiO_2)$ = 125 mg; T = 10 °C; Q_{air} = 5 L/h.

Table 5
Photocatalytic activity under UV–vis and Visirradiation of RE^{3+}–TiO_2 photocatalysts.

Sample label	Phenol degradation rate constant under UV–vis irradiation (h^{-1})	Phenol degradation rate constant under vis irradiation ($\lambda > 420$ nm) (h^{-1})
TiO_2_Pure_HT	2.4	0.16
TiO_2_Y(0.25)_HT	3.85	0.12
TiO_2_Pr(0.25)_HT	2.46	0.11
TiO_2_Er(0.25)_HT	2.81	0.23
TiO_2_Eu(0.25)_HT	2.73	0.23
TiO_2_Pure_SG	2	0.12
TiO_2_Y(0.5)_SG	1.55	0.26
TiO_2_Y(0.25)_SG	1.43	0.2
TiO_2_Pr(0.5)_SG	1.61	0.13
TiO_2_Pr(0.25)_SG	1.81	0.12
TiO_2_Er(0.5)_SG	1.72	0.18
TiO_2_Er(0.25)_SG	1.31	0.13
TiO_2_Eu(0.5)_SG	1.18	0.11
TiO_2_Eu(0.25)_SG	1.95	0.16
P25	2.75	0.09

ing pure TiO_2 and RE^{3+}–TiO_2 during vis ($\lambda > 420$ nm) or UV–vis illumination is presented in Fig. 7a,b and c,d, respectively. The observed rate constants of pure TiO_2, P25 and RE^{3+}–TiO_2 are listed in Table 5. It was found that all RE^{3+}–TiO_2 revealed higher photocatalytic activity than P25 under visible light irradiation. The highest UV-mediated activity was observed for TiO_2 modified with yttrium ions obtained by HT method. Phenol degradation rate constant was 3.85 h^{-1} for TiO_2 modified with 0.25 mol.% of Y^{3+}, while for pure TiO_2 degradation rate constant equaled to 2.40 h^{-1}. Phenol degradation rate constant on SG-prepared TiO_2 modified with the same concentration of Y^{3+} (0.25 mol.%) was only 1.43 h^{-1}. All HT-synthesized RE^{3+}–TiO_2 showed higher photocatalytic activity under UV–vis irradiation than that of pure TiO_2 obtained by the same method. However, the photocatalytic activity of RE^{3+}–TiO_2 prepared by SG method was lower than that of TiO_2_Pure_SG. Modification with yttrium was the most favorable under visible light irradiation for phenol degradation.

It should be pointed out that Er- and Eu-modified samples prepared by HT process revealed higher photocatalytic activity than bare titania prepared by the same method under both irradiation ranges. Moreover, Y- and Pr-modified titania samples showed higher and lower photocatalytic activity than bare titania under UV–vis and vis irradiation, respectively. At present, it is unclear if photoluminescence properties influenced resultant photocatalytic activity since the highest quenching of luminescence under 355 nm laser irradiation was observed for HT-sample: Er-modified TiO_2 (as shown in Fig. 5b).

Rate constant of phenol degradation was 0.26 h^{-1} under visible light for SG-prepared TiO_2 modified with 0.5 mol.% of Y. Photodegradation efficiency decreased with the decrease in the yttrium loading (0.25 mol.%) up to 0.2 h^{-1} proving that Y^{3+} was directly responsible for observed activity under visible light. Similar data were obtained for titania modified with Pr^{3+} and Er^{3+}, i.e., increase in photoactivity with increase of metal amount. However, contradictory results were achieved for Eu^{3+} modified titania, where the highest activity was obtained for lower amount of loaded metal (0.25 mol.%), and titania loading with larger amount of europium (0.5 mol.%) resulted in decrease in activity (the resultant activity was even slightly worse than that of bare titania). It is possible that large amount of surface-adsorbed carbon (the largest detected by XPS for this sample, as shown in Table 3) caused either worsening of efficient light absorption by "inner-filter effect" (photoabsorption by carbon compounds instead of Y^{+3}–TiO_2 and/or Y_2O_3) or when the carbon/doping concentration is too high, the presence of it can act as recombination centers [58].

The effect of RE^{3+} kind was different in the case of SG and HT methods. Er^{3+} and Eu^{3+} modified TiO_2 obtained by HT method was found to be most active in the phenol degradation (phenol degradation rate constant: 0.23 h^{-1}). While, in the case of SG method Y^{3+} modified titania was the most active. Photocatalysts prepared by HT method showed higher activity under UV–vis and, in some cases under vis irradiation compared to RE^{3+}–TiO_2 synthesized by SG method. Thus, as it was predicted, the preparation procedure strongly affected the photocatalytic activity of RE–TiO_2.

A clear correlation between BET surface area and photocatalytic activity was not observed, however, the TiO_2_Y(0.5)_SG sample of the largest surface area also showed the highest activity in phenol degradation under visible light irradiation. Photocatalysts prepared by HT method had higher both BET surface area and photocatalytic activity under UV light irradiation compared to TiO_2_Pure_HT. While, SG-prepared samples possessed higher BET surface area and lower photocatalytic activity under UV light irradiation than that of pure TiO_2, what could misleadingly suggest that a well-developed surface area is not beneficial in the case of photocatalytic activity under UV light irradiation. It must be pointed that specific surface areas of all these samples (HT and SG) were very high (two–three times higher than that of P25). Therefore, it was expected that reagents (oxygen, phenol) should adsorb efficiently on the surface of photocatalysts and specific surface area could not be reaction limiting factor. Reference experiments of phenol adsorption after 1 h stirring in the dark did not indicate its stable adsorption on pure and RE-modified TiO_2 confirming that specific surface area did not have significant impact on photocatalytic activity of these samples.

The results of this study agree with our previous findings that RE^{3+}–TiO_2 prepared by the sol–gel method revealed lower and higher photocatalytic activity under UV and vis light irradiation, respectively, compared to pure TiO_2 [24]. Moreover, similar results of photoactivity enhancement for RE^{3+}–TiO_2 prepared by HT method was reported by Obregon et al. [59]. It was presented that erbium-modified TiO_2 materials exhibited high photocatalytic activity for the liquid-phase degradation of phenol and methylene blue dye and the gas-phase degradation of toluene under both vis and UV light irradiation.

4. Mechanism discussion

In order to identify the possible mechanism of photocatalyst excitation under visible light, photocatalytic activity of the Pr–TiO_2 prepared by both methods, was investigated as a function of irradiation wavelength. Action spectra (AS) analysis demonstrates which fraction of absorbed light by photocatalyst, takes part in photocatalytic reaction. The AS results for the TiO_2_Pr(0.25)_SG and TiO_2_Pr(0.25)_HT samples are presented in Fig. 8. The samples with 0.25 mol.% of Pr^{3+} were selected for the measurements because praseodymium ions show the absorption bands near the TiO_2 absorption edge (Pr^{3+} max absorption peak at 446, 470 and 487 nm). Though Pr^{3+}–TiO_2 samples showed action spectra that did not resemble exactly the respective absorption spectra (measured as K–M function), it is clear that irradiation at range from 420 to 450 nm is responsible for photocatalytic activity under visible light (cross-hatching area of Fig. 8). The excitation of praseodymium $^3H_4$ ground state to the excited states of $^3P_2$ should be responsible for this activity. The lack of detectable activity for longer irradiation wavelengths of 450–490 nm indicates that other excited states of praseodymium do not participate in titania activation. Photocatalytic activity under visible light irradiation in reaction of acetic acid degradation for both photocatalysts was almost the same, similar as it was observed for phenol photodegradation (Fig. 7a).

Various mechanisms of organic compounds degradation under UV and visible light irradiation after modification with RE elements

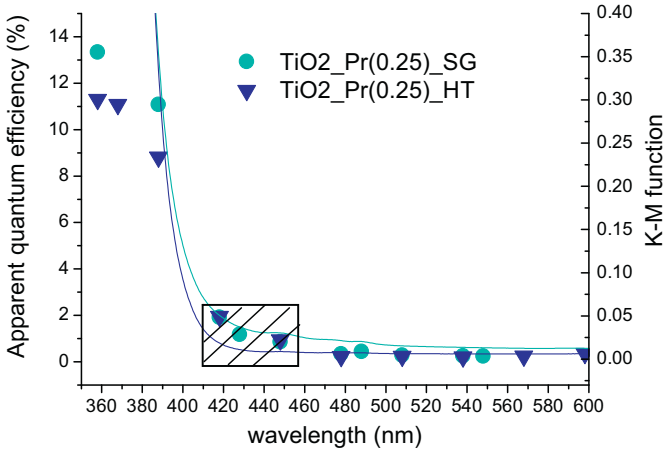

Fig. 8. Action spectrum of acetic acid oxidation on praseodymiummodified TiO_2 prepared by sol–gel and hydrothermal methods and absorption spectrum of samples.

have already been proposed. Albuquerque et al. [60] studied the effects of Ce-modification on the electronic and reduction properties of the TiO_2 anatase [60] facet using the mathematic calculations model. The natures of reduced Ce^{3+} and Ti^{3+} centers were investigated for different positions of dopant and oxygen vacancy on titania surface. It was found that the presence of the Ce dopant on the surface or subsurface caused a significant decrease in the surface energy and a slight decrease in the band gap through the introduction of empty Ce $4f^0$ states below the conduction band of anatase. It was reported that the most stable location for the Ce atom was at the outermost position, indicating that migration of the dopant from the bulk to the surface was thermodynamically favorable. Moreover, it was shown that the formation of oxygen vacancies was favored by the presence of the dopant on a subsurface position [60].

Our research confirms the mathematical model presented by Albuquerque et al. [60]. It is known that the ionic radiuses of Pr^{3+} (99 pm) and Eu^{3+} (95 pm) are larger than that of Y^{3+} (93 pm) and Er^{3+} (88 pm). The larger ionic radius is, the more thermodynamically favorable is migration to the surface during photocatalysts preparation, which results in formation of more RE^{3+} oxides on the surface (7th column in the Table 3). HT method of synthesis leads to decrease in migration process and lower amount of RE_2O_3 on the TiO_2 surface is detected (Table 4). It should be pointed that RE_2O_3 can also act as recombination center like many other dopants and surface modifiers, e.g., carbon, nitrogen, sulfur [58], boron [61]. In this regard, reduced photoactivity after titania SG-modification with RE under UV could be caused by enhancement of charge carriers recombination. Photocatalysts prepared by HT method have higher activity under UV irradiation, less RE oxides (RE_2O_3) and more OH^- species on the TiO_2 surface compared to powders obtained by SG method (Table 4). The OH^- groups on the TiO_2 surface result from H_2O dissociation at oxygen vacancy defects. Oxygen vacancies and surface defects can act as electron trapping sites, accelerating the separation of photogenerated electron–hole pairs. This explains the higher UV–vis photocatalytic activity of RE–TiO_2 prepared by HT method (possessing larger amount of oxygen and OH^- groups in the surface layer, as shown in Tables 3 and 4) than that of pure TiO_2 and TiO_2 modified by SG method. Luminescence properties (under irradiation with 355 nm) confirmed our observations, i.e., materials prepared by HT method showed lower emission intensity under UV excitation than those obtained by SG technique. This indicates that method of RE–TiO_2 synthesis has an impact on electron–hole recombination processes and HT method of RE–TiO_2 preparation allows better separation of charge carriers than SG technique (Fig. 5).

As was expected, under excitation at 250 nm, high intensity of luminescence of RE–TiO_2 prepared by HT method was not observed, due to existence of OH^- groups on the TiO_2 surface layer, which are known from their effective quenching properties. In addition, no correlation between luminescence intensity and photocatalytic activity was noticed. Though, photocatalysts prepared by HT method showed higher photocatalytic activity under visible light compared to those synthesized by SG method, the intensities of their luminescence emissions were lower.

Addition of RE element caused increase in the content of Ti^{3+} (Table 4, 3rd column) indicating increase of surface defect in TiO_2 structure. Photocatalysts prepared by HT method possessed more surface defects than that prepared by SG method. Created surface defects and oxygen vacancies can act as electron trap sites, accelerating the separation of photogenerated electron–hole pairs [62], and thus improving the photocatalytic activity under UV and visible light irradiation. Schematic representation of the dependence of preparation methods (HT, SG) on the surface composition and electron–hole recombination processes is presented in Fig. 9.

The most active sample under visible light irradiation, TiO_2_Y(0.5)_SG, was obtained by titania modification with 0.5 mol.% of yttrium, and possessed titania in the form of anatase, surface area of 151 m^2/g, and average crystals size of ca. 9 nm. It was found

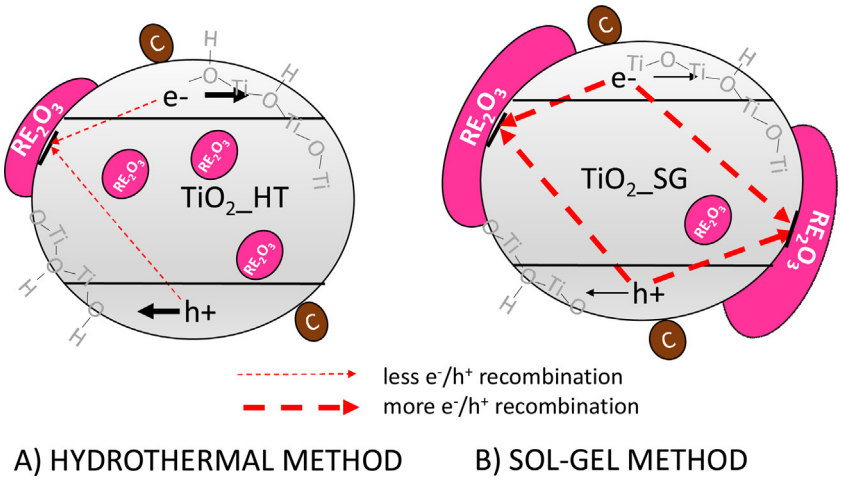

Fig. 9. Schematic representation of the dependence of preparation method on the surface composition and electron–hole recombination processes under UV light irradiation (A) hydrothermal method, (B) sol–gel method.

that this sample had the largest amount of oxygen in the form of TiO_2 (75.1%), and one of the lowest contents of carbon (23 wt%) on the surface of TiO_2. Described sample contained lower amount of RE_2O_3, Ti^{3+} and OH^- group but higher amount of TiO_2 on the surface layer compared to other TiO_2 modified with Y^{3+}. The absorption band for this sample showed the blue shift compared to pure TiO_2 prepared by the same procedure. XRD and XPS analyses of this sample indicate that Y^{3+} ions are rather in the form of their oxides, than in the form of cations in TiO_2 structure. Though the presence of Y_2O_3 on the surface of titania is responsible for its activation towards visible light, it can probably also act as an electron–hole recombination center, thus leading to decrease in photoactivity under UV–vis irradiation.

Summarizing, the primary mechanisms for photocatalytic activity for RE^{3+}–TiO_2 under UV and vis irradiation are different. Under UV light irradiation TiO_2 is excited and photogenerated electrons and holes migrated to its surface. RE_2O_3 acts as recombination center and OH^- group as electron trapping sites. While, under visible light irradiation titania cannot be excited due to its broad band-gap. Action spectra analysis showed that RE^{3+}-modified TiO_2 can be excited under visible light in the range from 420 to 450 nm. After TiO_2 modification with RE, the band gap of TiO_2 was enlarged. Thus, the excited electrons are more difficult to return to the VB, and the recombination of charge carriers was suppressed [63]. Therefore, it is proposed that RE–TiO_2 modification forms defects in the structure and surface of TiO_2. The free electrons can be captured at the defects. This process can greatly promote the separation of electrons and holes, contributing to enhanced photooxidation ability of holes (h^+). Meanwhile, the electrons are easier to react with oxygen molecules to generate another active species superoxide radical for the degradation of phenol.

5. Conclusions

The main conclusions of the study are described in points.

1. Addition of RE^{3+} ions during the sol–gel and hydrothermal syntheses of TiO_2 resulted in blue shift of absorption edges of TiO_2 and could be attributed to movement of conduction band edge above the first excited state of RE^{3+}. Incorporated RE^{3+} ions at the first excited state interact with the electrons of the conduction band of TiO_2, resulting in a higher energy transfer from the TiO_2 to RE^{3+} ions. However, observed blue shift could be also attributed to decrease in crystallite size of RE^{3+}–TiO_2 in comparison to TiO_2.
2. Incorporation of a small amount of RE elements into the TiO_2 structure increases the contraction of unit cell. RE ion is not able to replace Ti ion in TiO_2 lattice due to larger ionic radiuses of RE^{3+} ions than that of Ti^{4+}.
3. Luminescence properties (under 250 nm irradiation) of the samples as well as XRD and XPS analyses indicate that RE are rather in the form of their oxides than in the form of cations incorporated into the structure of TiO_2.
4. XPS analysis revealed the highest amounts of RE ions at the surface of Pr–TiO_2 and Eu–TiO_2 among all prepared samples. The ionic radiuses of Pr^{3+} (99 pm) and Eu^{3+} (95 pm) are larger than that of Y^{3+} (93 pm) and Er^{3+} (88 pm) and thus it can be a reason of their appearance on the surface of TiO_2 since larger ions are harder embedded into lattice structure. It is also seen that the sol–gel method is more favorable to congregate RE_2O_3 at the surface of TiO_2 when compared to the hydrothermal method.
5. All RE–TiO_2 samples prepared by the hydrothermal method have higher BET surface area and lower crystallite size compared to powders obtained by the sol–gel technique. On the other hand, photocatalysts prepared by the sol–gel method contained higher amount of RE_2O_3 on their surfaces, less number of OH^- groups and Ti^{3+} moieties than powders obtained via hydrothermal method.
6. All samples (Y^{3+}, Pr^{3+}, Er^{3+} and Eu^{3+} modified TiO_2) obtained by hydrothermal and the sol–gel methods showed higher activity under visible light irradiation compared to pure P25 TiO_2. However, all photocatalysts prepared by SG showed lower activity under UV–vis irradiation in comparison to pure TiO_2. OH^- groups on the TiO_2 surface layer prepared by HT enhance the photocatalytic activity both under visible and UV–vis irradiation and decrease the luminescence emission intensity (under 250 and 980 nm irradiation).
7. Action spectra analysis showed that RE^{3+}-modified TiO_2 can be excited under visible light in the range from 420 to 450 nm. The primary mechanism for the visible light sensitization was probably due of oxygen vacancies and OH^- groups which appeared on the TiO_2 surface layer.

Acknowledgements

This research was financially supported by Polish National Science Center (grant no. 2011/01/N/ST5/05537). The project was co-financed by the European Union within the European Social Fund.

Appendix A. Supplementary data

Supplementary data associated with this article can be found, in the online version, at http://dx.doi.org/10.1016/j.apcatb.2015.09.001.

References

[1] A. Rapsomanikis, A. Apostolopoulou, E. Stathatos, P. Lianos, J. Photochem. Photobiol. A 280 (2014) 46–53.
[2] M. Nischk, P. Mazierski, M. Gazda, A. Zaleska, Appl. Catal. B 144 (2013) 674–685.
[3] A. Zaleska, A. Hänel, M. Nischk, Recent Pat. Eng. 4 (2010) 200–216.
[4] A. Cybula, J.B. Priebe, M.-M. Pohl, J.W. Sobczak, M. Schneider, A. Zielińska-Jurek, A. Brückner, A. Zaleska, Appl. Catal. B 152–153 (2014) 202–211.
[5] J. Kuncewicz, P. Ząbek, G. Stochel, Z. Stasicka, W. Macyk, Catal. Today 161 (2011) 78–83.
[6] E. Grabowska, J. Reszczynska, A. Zaleska, Water Res. 46 (2012) 5453–5471.
[7] S.G. Ghugal, S.S. Umare, R. Sasikala, Mater. Res. Bull. 61 (2015) 298–305.
[8] A. Krukowska, J. Reszczynska, A. Zaleska, Physicochem. Probl. Miner. Process. 50 (2014) 551–561.
[9] A. Charanpahari, S.S. Umare, R. Sasikala, Appl. Surf. Sci. 282 (2013) 408–414.
[10] E. Grabowska, A. Zaleska, S. Sorgues, M. Kunst, A. Etcheberry, H. Remita, J. Phys. Chem. C 117 (2013) 1955–1962.
[11] E. Grabowska, J. Sobczak, M. Gazda, A. Zaleska, Appl. Catal. B 117–118 (2012) 351–359.
[12] M. Kralova, P. Dzik, M. Vesely, J. Cihlar, Catal. Today 230 (2014) 188–196.
[13] E. Kowalska, M. Janczarek, L. Rosa, S. Juodkazis, B. Ohtani, Catal. Today 230 (2014) 131–137.
[14] P. Sathishkumar, R.V. Mangalaraja, O. Rozas, H.D. Mansilla, M.A. Gracia-Pinilla, S. Anandan, Ultrason. Sonochem. 21 (2014) 1675–1681.
[15] M. Bellardita, A. Di Paola, L. Palmisano, F. Parrino, G. Buscarino, R. Amadelli, Appl. Catal. B 104 (2011) 291–299.
[16] S. Ramya, S.D. Ruth Nithila, R.P. George, D.N.G. Krishna, C. Thinaharan, U. Kamachi Mudali, Ceram. Int. 39 (2013) 1695–1705.
[17] Y. Xin, H. Liu, J. Solid State Chem. 184 (2011) 3240–3246.
[18] J.J. Xu, Y.H. Ao, D.G. Fu, C.W. Yuan, Colloids Surf. A 334 (2009) 107–111.
[19] H. Shi, T. Zhang, T. An, B. Li, X. Wang, J. Colloid Interface Sci. 380 (2012) 121–127.
[20] M. Saif, S.M.K. Aboul-Fotouh, S.A. El-Molla, M.M. Ibrahim, L.F.M. Ismail, Spectrochim. Acta Part A 128 (2014) 153–162.
[21] J. Castaneda, J. Rare Earths 29 (2011) 420–425.
[22] Q. Shang, H. Yu, X. Kong, H. Wang, X. Wang, Y. Sun, Y. Zhang, Q. Zeng, J. Lumin. 128 (2008) 1211–1216.
[23] U.G. Akpan, B.H. Hameed, Appl. Catal. A 375 (2010) 1–11.
[24] J. Reszczyńska, T. Grzyb, J.W. Sobczak, W. Lisowski, M. Gazda, B. Ohtani, A. Zaleska, Appl. Surf. Sci. 307 (2014) 333–345.
[25] X. Wang, B. Liu, Y. Yang, Opt. Laser Technol. 58 (2014) 84–88.
[26] J. Reszczyńska, T. Grzyb, J.W. Sobczak, W. Lisowski, M. Gazda, B. Ohtani, A. Zaleska, Appl. Catal. B 163 (2015) 40–49.

[27] E.I. Seck, J.M. Doña-Rodríguez, E. Pulido Melián, C. Fernández-Rodríguez, O.M. González-Díaz, D. Portillo-Carrizo, J. Pérez-Peña, J. Colloid Interface Sci. 400 (2013) 31–40.
[28] Z. Wei, E. Kowalska, B. Ohtani, Molecules 19 (2014) 19573–19587.
[29] M. Kavitha, C. Gopinathan, P. Pandi, Int. J. Adv. Res. Technol. 2 (2013) 102–108.
[30] B. Ohtani, O.O. Prieto-Mahaney, D. Li, R. Abe, Photochem. Photobiol. A 216 (2010) 179–182.
[31] R. Parra, M.S. Góes, M.S. Castro, E. Longo, P.R. Bueno, J.A. Varela, Chem. Mater. 20 (2007) 143–150.
[32] M. Pal, U. Pal, J.M. Jimenez, F. Perez-Rodriguez, Nanoscale Res. Lett. 7 (2012) 1.
[33] J.W. Shi, J.T. Zheng, P. Wu, J. Hazard Mater. 161 (2009) 416–422.
[34] J. Reszczynska, A. Iwulska, G. Śliwinski, A. Zaleska, Physicochem. Probl. Miner. Process. 48 (2012) 201–208.
[35] Y. Yang, C. Zhang, Y. Xu, X. Wang, X. Li, C. Weng, Mater. Lett. 64 (2010) 147–150.
[36] S. Obregón, G. Colón, Appl. Catal. B 152–153 (2014) 328–334.
[37] W. Su, J. Chen, L. Wu, X. Wang, X. Wang, X. Fu, Appl. Catal. B 77 (2008) 264–271.
[38] J. Yang, J. Dai, J. Li, Appl. Surf. Sci. 257 (2011) 8965–8973.
[39] J. Reszczynska, D. Arenas Esteban, M. Gazda, A. Zaleska, Physicochem. Probl. Miner. Process. 50 (2014) 515–525.
[40] R. Guo, Y.C. Wu, P.Z. Fu, F.L. Jing, Chem. Phys. Lett. 416 (2005) 133–136.
[41] C.-H. Liang, M.-F. Hou, S.-G. Zhou, F.-B. Li, C.-S. Liu, T.-X. Liu, Y.-X. Gao, X.-G. Wang, J.-L. Lü, J. Hazard. Mater. 138 (2006) 471–478.
[42] M. Grujic-Brojcin, S. Armakovic, N. Tomic, B. Abramovic, A. Golubovic, B. Stojadinovic, A. Kremenovic, B. Babic, Z. Dohcevic-Mitrovi, M. Scepanovic, Mater. Charact. 88 (2014) 30–41.
[43] C. Zhan, F. Chen, J. Yang, D. Dai, X. Cao, M. Zhong, J. Hazard. Mater. 267 (2014) 88–97.
[44] K.S. Kumar, C.-G. Song, G.M. Bak, G. Heo, M.-J. Seong, J.-W. Yoon, J. Alloys Compd. 617 (2014) 683–687.
[45] K.S. Kumar, J. Ayyappan, C. Venkateswaran, Mater. Res. Bull. 65 (2015) 224–230.
[46] P. Yan, H. Jiang, S. Zang, J. Li, Q. Wang, Mater. Chem. Phys. 139 (2013) 1014–1022.
[47] D.P. Birnie III, N.J. Bendzko, Mater. Chem. Phys. 59 (1999) 26–35.
[48] P. Piszczek, Polyhedron 26 (2007) 93–100.
[49] H. Ardelean, A. Seyeux, S. Zanna, F. Prima, I. Frateur, P. Marcus, Corros. Sci. 73 (2013) 196–207.
[50] T.N.P. Homhuan, T. Chikyow, S. Tungasmita, Jpn. J. Appl. Phys. 50 (2011) 10PA03.
[51] F.J. Knorr, J.L. McHale, J. Phys. Chem. C 117 (2013) 13654–13662.
[52] S. Kaniyankandy, H.N. Ghosh, J. Phys. Chem. 19 (2009) 3523–3528.
[53] K. Binnemans, C. Görller-Walrand, J. Rare Earths 14 (1996) 173–180.
[54] W. Chen, A.G. Joly, C.M. Kowalchuk, J.-O. Malm, Y. Huang, J.-O. Bovin, J. Phys. Chem. B 106 (2002) 7034–7041.
[55] F. Auzel, Chem. Rev. 104 (2004) 139–174.
[56] P.T. Nga, C. Barthou, P. Benalloul, P.N. Thang, L.N. Chung, P.V. Hoi, L.V. Luat, P.T. Cuong, J. Non-Cryst. Solids 352 (2006) 2385–2389.
[57] A.M. Kłonkowski, S. Lis, M. Pietraszkiewicz, Z. Hnatejko, K. Czarnobaj, M. Elbanowski, Chem. Mater. 15 (2003) 656–663.
[58] X.F. Lei, X.X. Xue, H. Yang, C. Chen, X. Li, J.X. Pei, M.C. Niu, Y.T. Yang, X.Y. Gao, J. Alloys Compd. 646 (2015) 541–549.
[59] S. Obregon, A. Kubacka, M. Fernández-García, G. Colón, J. Catal. 299 (2013) 298–306.
[60] A.R. Albuquerque, A. Bruix, J.R. Sambrano, F. Illas, J. Phys. Chem. C 119 (2015) 4805–4816.
[61] Y. Gong, C. Fu, L. Ting, J. Chenu, Q. Zhao, C. Li, Appl. Surf. Sci . 351 (2015) 746–752.
[62] A.L. Linsebigler, G. Lu, J.T. Yates, Chem. Rev. 95 (1995) 735–758.
[63] R. Cao, H. Huang, N. Tian, Y. Zhang, Y. Guo, T. Zhang, Mater. Charact. 101 (2015) 166–172.